J. Neural Eng. **4** (2007) 159–172 doi:10.1088/1741-2560/4/2/015

Microfluidic engineered high cell density three-dimensional neural cultures

D Kacy Cullen[1], Jelena Vukasinovic[2], Ari Glezer[2] and Michelle C LaPlaca[1]

[1] Wallace H Coulter Department of Biomedical Engineering, Parket H Petit Institute for Bioengineering and Bioscience, Laboratory for Neuroengineering, Georgia Institute of Technology, Atlanta, GA, USA
[2] George W Woodruff School of Mechanical Engineering, Georgia Institute of Technology, Atlanta, GA, USA

E-mail: dkacy@neuro.gatech.edu, jelena.vukasinovic@me.gatech.edu, ari.glezer@me.gatech.edu and michelle.laplaca@bme.gatech.edu

Received 14 December 2006
Accepted for publication 28 February 2007
Published 4 April 2007
Online at stacks.iop.org/JNE/4/159

Abstract

Three-dimensional (3D) neural cultures with cells distributed throughout a thick, bioactive protein scaffold may better represent neurobiological phenomena than planar correlates lacking matrix support. Neural cells *in vivo* interact within a complex, multicellular environment with tightly coupled 3D cell–cell/cell–matrix interactions; however, thick 3D neural cultures at cell densities approaching that of brain rapidly decay, presumably due to diffusion limited interstitial mass transport. To address this issue, we have developed a novel perfusion platform that utilizes forced intercellular convection to enhance mass transport. First, we demonstrated that in thick (>500 μm) 3D neural cultures supported by passive diffusion, cell densities $\leqslant 5.0 \times 10^3$ cells mm^{-3} were required for survival. In 3D neuronal and neuronal–astrocytic co-cultures with increased cell density ($\geqslant 10^4$ cells mm^{-3}), continuous medium perfusion at 2.0–11.0 μL min^{-1} improved viability compared to non-perfused cultures ($p < 0.01$), which exhibited widespread cell death and matrix degradation. In perfused cultures, survival was dependent on proximity to the perfusion source at 2.00–6.25 μL min^{-1} ($p < 0.05$); however, at perfusion rates of 10.0–11.0 μL min^{-1} survival did not depend on the distance from the perfusion source, and resulted in a preservation of cell density with >90% viability in both neuronal cultures and neuronal–astrocytic co-cultures. This work demonstrates the utility of forced interstitial convection in improving the survival of high cell density 3D engineered neural constructs and may aid in the development of novel tissue-engineered systems reconstituting 3D cell–cell/cell–matrix interactions.

Introduction

Three-dimensional (3D) cell culture systems allow investigation of cellular behavior in a more physiologically relevant state while preserving the primary advantages of traditional two-dimensional (2D) *in vitro* systems, such as control of cellular environment, accessibility for repeated imaging and elimination of systemic effects. Cells cultured in a 3D environment have been shown to better represent *in vivo* cellular behavior than cells cultured in monolayer (e.g., osteoblastic cells (Granet *et al* 1998), fibroblasts (Grinnell 2000), breast epithelial cells (Wang *et al* 1998) and neurons and astrocytes (Fawcett *et al* 1989, 1995)). Fundamental differences exist between cells cultured in monolayer versus 3D configurations in terms of access to soluble factors and the distribution and types of cell–cell and cell–extracellular matrix (ECM) interactions (Cukierman *et al* 2001, Cukierman *et al* 2002, Schmeichel and Bissell 2003, Yamada *et al* 2003). Cell–cell and cell–ECM interactions may be constrained or completely omitted in planar cultures. Furthermore, culture models consisting of multiple cell types closer approximate the heterogeneity of *in vivo* tissue. With respect to the nervous system, cellular heterogeneity is important to represent such interactions as physical support

 © 2007 IOP Publishing Ltd Printed in the UK

and metabolic coupling between neurons and astrocytes (Tsacopoulos and Magistretti 1996, Aschner 2000, Tsacopoulos 2002).

Neural cell culture models have been developed to approximate a 3D orientation by plating dissociated primary cells above a matrix material (Coates and Nathan 1987, Coates *et al* 1992, O'Shaughnessy *et al* 2003). Such systems may support high 2D cell densities, although cell–cell and cell–matrix interactions are constrained as cells are not distributed throughout the full thickness of the matrix. Reaggregate neural cultures have been developed by rotation-induced reassociation (Hsiang *et al* 1989, Choi *et al* 1993, Spector *et al* 1993). These systems produce 3D spheres at high cell densities via diffusion with convective enhancement of circulating medium; however, the volume available for growth is inherently limited based on required surface area to volume ratios that permit survival, thus limiting the scope of 3D interactions. Other systems have been developed with cells distributed throughout a matrix material (Bellamkonda *et al* 1995a, 1995b, Woerly *et al* 1996, O'Connor *et al* 2000, 2001, Cullen *et al* 2006). However, these cultures have relied solely on passive diffusion for nutrient delivery and waste product removal, necessitating the use of cell densities much lower than those found in the brain. Thus, technical limitations have prevented the development of 3D neural cell culture models consisting of a high cell density ($\geqslant 10^4$ cells mm^{-3}) with greater than millimeter scale dimensions and full thickness cellular distribution.

More biologically accurate 3D cell–cell and cell–matrix interactions may be represented by thick, high cell density neural preparations; however, these parameters are in direct competition with providing a sufficient supply of nutrients and oxygen to the cells. The most common systems to address this issue are spinner flasks and rotating vessels; however, both systems enhance diffusion via increased fluid flow around a 3D construct, rather than using perfusion for direct forced convection through a construct. In non-neural systems, perfusion bioreactors have been developed for a range of tissue engineering applications. In general, the goals of these systems are to enhance survival in thick and/or high cell density systems (e.g., thick osteoblast constructs (Cartmell *et al* 2003), high density (10^5 cells mm^{-3}) hepatoblastoma cell line (Hongo *et al* 2005) and hepatocytes (Toh *et al* 2005)), as a mechanism to improve cell seeding into porous scaffolds (e.g., bone marrow stromal cells (BMSCs) (Wang *et al* 2006)), to introduce hydrodynamic shear stress to enhance cell differentiation or improve productivity (e.g., BMSCs (Gomes *et al* 2003, Holtorf *et al* 2005), bone marrow-derived osteoblasts (van den Dolder *et al* 2003, Wang *et al* 2003), bovine chondrocytes (Cooper Jr *et al* 2007)), or some combination of these general parameters (e.g., hepatocytes (Chen and Lin 2006), chondrocytes (Saini and Wick 2003) and NIH/3T3 cells (Kitagawa *et al* 2006)).

Previous work related to culture perfusion in the field of neurobiology has focused on maintaining the viability of acute brain slices during physiological studies using continuous circulation of the nutrient medium, and diffusion and/or capillary action-limited mass transport in nutrient delivery. For example, in one type of system tissue rests on a mesh at the interface between an open channel flow of perfusate underneath the mesh and the humidified atmosphere of gases above the mesh (Li and McIlwain 1957, Haas *et al* 1979, Reynaud *et al* 1995). In these interface-type chambers, only one side of the tissue is exposed to the media with intercellular nutrient concentration being limited by capillary action and diffusion. In another approach, a slice is entirely submerged in the culture medium and perfused using oxygenated media (Nicoll and Alger 1981, Zbicz and Weight 1985, Shi and Bunney 1990). These submerged-type chambers enable faster diffusion into the slice than interface-type chambers, where only one side of the tissue is exposed to media. Both chamber arrangements have practical advantages and shortcomings; however, submerged tissue generally obtains a more stable environment as a gas–liquid interface may lead to discontinuities in the flow of media and gas due to surface tension-induced pulsations. Accordingly, reduced disruption of ionic homeostasis by anoxia in rat hippocampal slices has been reported in submerged slices (Croning and Haddad 1998). However, the transport mechanisms in submerged- or interface-type chambers inherently restrict the long-term utility of these devices in meeting cellular metabolic demands; thus the tissue ultimately decays.

The goal of this study was to develop and validate a novel engineered neural cell culture system with the following attributes: (1) the use of 3D cell–cell and cell–matrix interactions throughout a large, thick, dense neural culture, (2) control of cell population, ranging from a nearly pure neuronal population to neurons and astrocytes mixed in a controlled ratio and (3) the ability to increase 3D cell density to more realistically approximate that of brain. The latter point was accomplished using a custom-designed bioreactor perfusion system utilizing forced convection to continuously deliver nutrients and withdraw waste from thick constructs. In the current study, we initially identified neural cell density ranges where passive diffusion was insufficient to satisfy cellular metabolic needs. We then demonstrated that forced convection, interstitial nutrient delivery was sufficient to meet the cellular metabolic requirements throughout thick, high cell density neural constructs. This bioreactor perfusion system maintains sufficiently high concentrations of nutritive substances throughout thick, high cell density neural constructs, and thus may be a valuable platform for a range of neurobiological as well as neural tissue engineering applications.

Materials and methods

Isolation of neurons (embryonic day 17–18) and astrocytes (postnatal day 0–1)

Neurons were isolated from timed-pregnant (E17–18) Sasco Sprague-Dawley rats (Charles River, Wilmington, MA), which were anesthetized using isoflurane and decapitated. The uterus was removed by caesarian section and placed

in Hanks balanced salt solution (HBSS). Each fetus was removed from the amniotic sac, rapidly decapitated, and the brains removed. The cerebral cortex was isolated and the hippocampal formation removed. To dissociate the tissue, pre-warmed trypsin (0.25%) + 1 mM EDTA was added for 10 min at 37 °C. The trypsin–EDTA was then removed and deoxyribonuclease I (0.15 mg mL^{-1}, DNase) in HBSS was added. The tissue was then tritutated with a flame-narrowed Pastuer pipet and centrifuged at 200 g for 3 min after which the supernatant was aspirated and the cells were resuspended in neuronal media (neurobasal medium + 2% B-27 + 500 μM L-glutamine). Similar procedures have previously been demonstrated to yield a nearly pure neuronal population, with glial contamination less that 1% (Brewer *et al* 1993, Brewer 1995).

Astrocytes were acquired from postnatal (day 0–1) Sasco Sprague-Dawley rats (Charles River) anesthetized using isoflurane and rapidly decapitated. The brain was removed and the cerebral cortices isolated as described above. Cortices were minced and placed in pre-warmed trypsin (0.25%) + EDTA (1 mM) at 37 °C for 5 min. DNase was added and the tissue was triturated using a flame-narrowed Pasteur pipet. Medium was added (DMEM/F12 + 10% FBS) and the cells were centrifuged (200 g, 3 min) after which the supernatant was aspirated, the cells were resuspended in DMEM/F12 + 10% FBS and transferred to tissue culture flasks. Astrocytes were passaged to isolate a nearly pure population of type I astrocytes as previously described (McCarthy and de Vellis 1980). Briefly, at various time points over the first week post-dissection, the flasks were mechanically agitated to dislodge less adherent cell types. As the cells approached ~90% confluency, they were resuspended using trypsin–EDTA, centrifuged and replated at a density of 300 cells mm^{-2}. Astrocytes were used in 3D culture between passages 4–12 to permit cell maturation and to acquire a nearly pure astrocytic population (>95%, as assessed by glial-fibrillary acidic protein immunoreactivity). Astrocytes were re-suspended in co-culture medium (neurobasal + 2% B-27 + 1% G-5 + 500 μM L-glutamine) for plating in 3D culture.

All procedures involving animals were approved by the Institutional Animal Care and Use Committee of the Georgia Institute of Technology. All cell culture reagents were from Invitrogen (Carlsbad, CA) or Sigma (St Louis, MO) unless otherwise specified.

3D neuronal cultures and neuronal–astrocytic co-cultures

Cultures consisting of a nearly pure neuronal population (neuronal cultures) or neurons mixed with astrocytes at a 1:1 ratio (neuronal–astrocytic co-cultures) were cultured within Matrigel® matrix (final protein concentration of 7.5 mg mL^{-1}; BD Biosciences; Bedford, MA). Matrigel® exhibits fluid-like behavior at 4 °C (which permits even dispersion of dissociated cells throughout the matrix) and subsequent gelation at or near physiological temperature (which entraps cells in 3D matrix) (Kleinman *et al* 1986). Cultures were placed at 37 °C to permit matrix gelation and 3D cell entrapment, after which 0.5 mL of the appropriate medium was added. Cultures were maintained at 37 °C and 5% CO_2-95% humidified air. Neuronal cultures were plated at a cell density range of 1.25–2.50, 3.75–5.00, 6.25–7.50 and 10.0–12.5 × 10^3 cells mm^{-3} in custom-made culture chambers consisting of a glass coverslip below a circular (15.7 mm diameter) polydimethysiloxane (PDMS; Sylgard 184 and 186, Dow Corning, Midland, MI) mold and fed at 1 and 4 days *in vitro* (DIV). Culture viability was assessed at 2 and 7 DIV (n = 4–12 per condition per time point). Neuronal and neuronal–astrocytic co-cultures were plated in custom perfusion chambers at 10^4 cells mm^{-3} (corresponding to 2 × 10^6 cells) with viability assessed at 2 DIV (see below). For perfusion studies, culture medium was supplemented with a 1% antibiotic/antimycotic solution.

Perfusion bioreactor design

Perfusion platforms (patent pending) consisted of an inner, culture chamber with 3D intercellular nutrient convection; an outer, inclined collecting pool; inlet and outlet ports (figure 1) (Vukasinovic and Glezer 2006a, 2006b). Using a syringe pump having opposing syringes on a single drive (KdScientific KDS260), continuous infusion of nutrients through the inlet port was kept in mass equilibrium with the amount of retrieved perfusate (containing depleted media and catabolites) from the outlet port. The inner, cylindrical culture chamber was an aerated and perfused media bath, bound with perfusion substrate at its base and an optically transparent membrane at its top. It measured 15.7 mm in diameter and 3 mm in height. PDMS perfusion substrate contained an array of nine circular Au grids (PELCO®). Grids measured 3 mm in diameter and contained 54 μm × 54 μm openings to permit medium entry through approximately 40% of their surface. The culture chamber and outer pool were connected by peripheral microchannel exits (starting 300 μm above the perfusing substrate) that enabled withdrawal of perfusate from the culture chamber. The culture chamber and collecting pool were encapsulated by a selectively permeable membrane stretched over a Teflon holder and sealed by O-rings. The membrane is permeable to gases necessary for cell metabolism and impermeable to microbes and water vapor, thereby ensuring that the culture was moist, well aerated and at physiological pH in a sterile environment at a reduced risk of cross-contamination (Potter and DeMarse 2001).

Perfusion bioreactor fabrication

Perfusion platforms were fabricated using a simple and inexpensive method that combines 3D solid object printing (McDonald *et al* 2002) and soft lithography (Xia and Whitesides 1998, McDonald *et al* 2000, Whitesides *et al* 2001). Solid object printing (SOP) is an inkjet printing tool that rapidly produces robust, 3D physical models from 3D CAD drawings (figure 2(a)) by spraying layers of tiny droplets of a non-toxic thermopolymer material onto a platform surface. A solid object printer (ThermoJet 2000, 3D Systems) extruded disposable masters with a feature resolution of 300 × 400 × 600 dpi in x, y and z, respectively (figure 2(b)). This printed disposable template was then used for replica molding of the

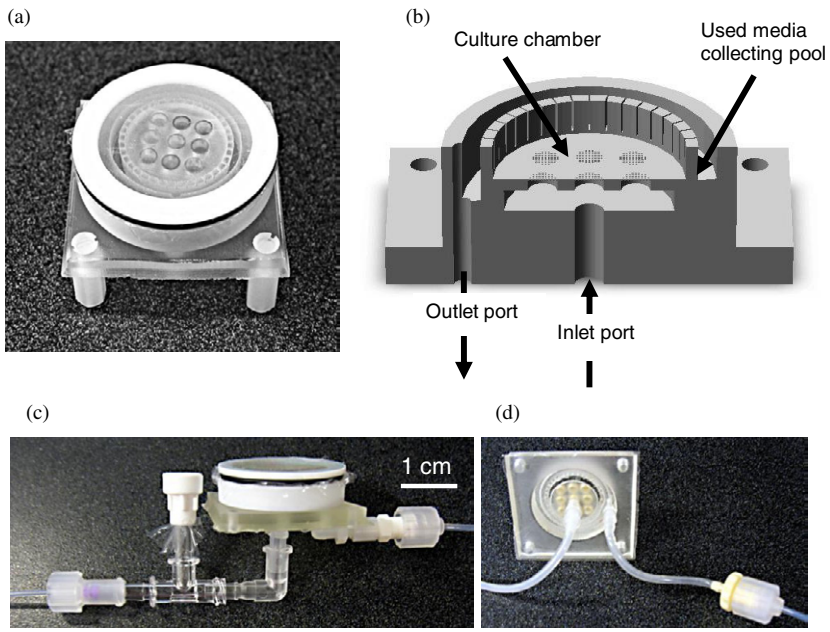

Figure 1. Cultures were contained within custom PDMS culture chambers (580 μL total volume). Perfusion platform with attached FEP membrane (permitting gas exchange without loss of water vapor) in a Teflon holder that encapsulates the device (a). Cross section view of the PDMS perfusion platform showing a centrally formed, perfused culture chamber; inlet and outlet ports (b). Cylindrical culture chamber is comprised of nine Au grids embedded into the base to deliver the nutrient medium, and peripheral microchannel exits through which spent media and catabolites leave the chamber. Perfusion platform using appropriate fittings and tubing (c), (d).

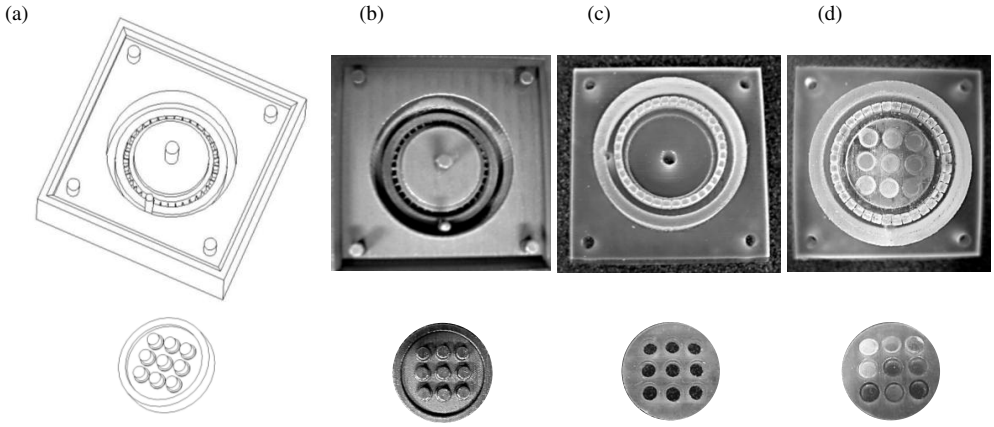

Figure 2. Fabrication methodology: CAD design of the perfusion chamber and the perfusing substrate mold (a), printed 3D thermopolymer molds (b), replica molded perfusion chamber and perfusing substrate in PDMS (c), Au grids sealed to the perfusing substrate, and perfusing substrate sealed to the perfusion chamber (d).

perfusion chambers using PDMS (figure 2(c)), which was poured into the template, cured at room temperature for 48 h and peeled off (figure 2(c)). The use of mold release agents was deemed unnecessary owing to the favorable surface chemistries of materials in contact. Separate disposable molds were fabricated for the replica molding of the 3D perfusion structure substrate (figures 2(a), (b)). Injection sites consisted of nine Au grids sealed to the perfusing/cell attachment substrate via thin layer of contact-sealing PDMS prepolymer and catalyst mixture yielding a watertight bond, and the perfusion substrate sealed to the perfusion chamber using the same approach (figure 2(d)). The perfusion platform and all associated components were autoclaved prior to cell culture.

Flow diagnostics

The induced flow within the culture chamber was investigated experimentally using microscopic particle image velocimetry (μ-PIV) (Santiago *et al* 1998, Wereley and Meinhart 2004). This non-intrusive technique obtains reliable 2D velocity fields in planes parallel to the perfusing substrate by adjusting the distance between the perfusion chamber and imaging optics. Fluid velocity was measured by recording the displacement of 550 nm fluorescent tracer particles added

to the fluid under the assumptions that the particle density was commensurate to that of the fluid and that the particles were small enough to faithfully follow, but not influence, the flow. The experimental setup consisted of an upright microscope in episcopic, darkfield, fluorescence arrangement and a high-intensity halogen illuminator. Darkfield illumination improves particle visibility by enhancing particle-to-background contrast. Particle fluorescence was captured by an 8-bit CCD monochrome camera upon relevant filtering.

Standard PIV algorithms estimated the local fluid velocity based on successive images of the seed particles at a known, sufficiently short time-delay between the captured frames. For sub-millimeter scale field-of-view, additional routines were developed to supplement these algorithms to reduce uncertainties in local velocity measurements due to diffusion, low particle seeding density and the overall particle ability to accurately follow the flow (Vukasinovic and Glezer 2006a, 2006b). In μ-PIV, measurement depth depends on the depth of focus of the diffraction-limited imaging optics, the resolving power of the detector (pixel size for a CCD chip), and the finite size of particles, as some out-of-focus particles were still sufficiently bright to contribute to the correlation function applied for the PIV interrogation analysis (Meinhart *et al* 2000a). To limit the noise associated with non-zero background intensity in the correlation plane and facilitate the search for in-focus particles, the background level was brought close to zero by subtracting the mean background intensity from all acquired images. A high-pass filter was applied to threshold such images and reject the out-of-focus, larger, dimmer particles. True, zero-background images were then appropriately gained to enhance the visibility of remaining particles and raise the relative strength of the correlation peak in subsequent processing (Bolinder 1999). Particle images, sampled at statistically independent times, were appropriately overlapped to increase the image seeding density while maintaining the actual concentration low to prevent the clogging of perfusion chambers (Meinhart *et al* 2000b). Such well-seeded particle image pairs were then fed to the PIV interrogation software to extract the steady, laminar velocity distributions. This approach facilitates the search for the cross-correlation peak by increasing the number of particles per interrogation window and reduces diffusive uncertainty. Directionally unbiased error associated with Brownian motion was therefore negligible for velocity estimates based on about ten particles per interrogation window and averaging over hundreds of instantaneous realizations (within 0.3%). Overall, the estimated velocity resolution is within 5% of the microjet ejection velocity.

Culture perfusion

Neuronal cultures and neuronal–astrocytic co-cultures were exposed to continuous medium perfusion at flow rates of 0.30–1.00, 2.00–2.50, 5.00–6.25, 10.0–11.0 μL min^{-1}; non-perfused control cultures had media changed daily (n = 3–11 per culture type per condition). Flow rates are presented based on total volumetric flow through a construct; however, convective exchange rates are presented in table 1 based on complete medium changes of entire culture volume (580 μL; cellular constructs were 200 μL). The level of the bathing medium within the culture chamber was controlled externally by timing the start of suction, ensuring that the entire volume of the culture chamber (containing the 500–750 μm thick submerged 3D neural cultures) was bathed in medium prior to the start of the continuous, closed-loop circulation. Matrigel® matrix remained adherent to the perfusion substrate throughout experimentation. Medium was injected into the culture chamber normal to the perfusing substrate via the arrays of microjets. The intercellular convection was predicted to follow the induced, 3D flow pattern within the culture chamber through microjet interactions and peripheral perfusate extraction via 36 microchannels (each measuring 150 μm in width) that were formed in the cylindrical enclosure bounding the perimeter of the cultures (figure 3). Used media and metabolic waste leaving the culture chamber through the microchannels was collected in the outer pool and exited the perfusion platform through the outlet port.

Table 1. Summary of cell culture and perfusion parameters. The number of complete media changes per day was calculated based on reservoir volume.

Culture parameters		Perfusion parameters			
Culture volume	Reservoir volume	μL min^{-1}	μL h^{-1}	mL/day	Number of exchanges/day
200 μL	580 μL	1.00	60	1.4	2.5[a]
		2.50	150	3.6	6.2[a]
		6.25	375	9.0	15.5[a]
		11.0	660	15.8	27.3[a]

[a] Based on reservoir volume.

Viability/cytotoxicity assay, image acquisition and statistical analysis

Following neural cell density and perfusion studies, cells were labeled using fluorescent probes for distinguishing live and dead cells (LIVE/DEAD Viability/Cytotoxicity Kit; Molecular Probes). Cell cultures were incubated with calcein AM (2 μM) and EthD-1 (4 μM) at 37 °C for 30 min and rinsed with 0.1 M Dulbecco's phosphate-buffered saline (DPBS). Cell cultures were viewed using a laser scanning confocal microscope (LSM 510, Zeiss, Oberkochen, Germany). Multiple z-stacks were acquired across the full thickness of each culture. For statistical analysis, $\geqslant$3 regions were sampled per culture, except in cases of complete culture degeneration where a single representative region was acquired. Images were analyzed using a LSM image browser (Zeiss). Where observed, live cells (calcein^{+}; fluorescing green via AM-cleavage) and cells with compromised membranes (EthD-1^{+}; nuclei fluorescing red by EthD-1 binding to DNA) were manually counted and the percentage of viable cells was calculated. Dead cells (EthD-1^{+}) that exhibited a degenerating morphology consisting of punctuated body formation and condensed nuclear material were also quantified as a function of culture height and, hence, distance from the perfusion source. All confocal

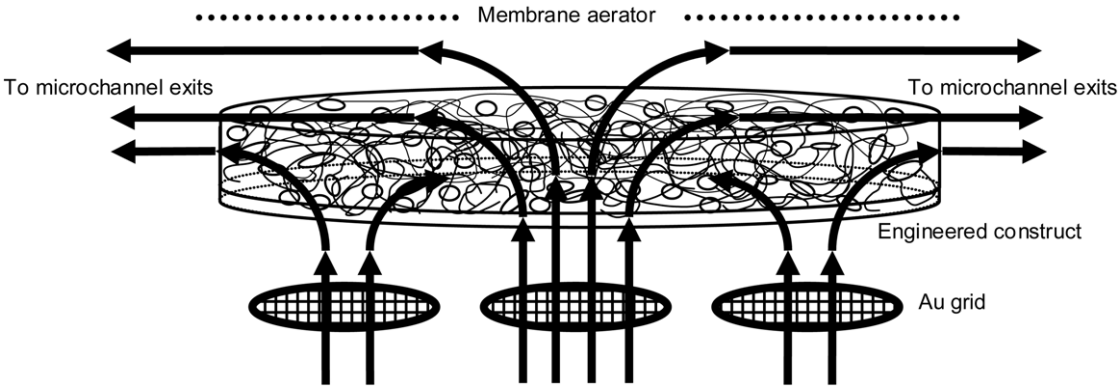

Figure 3. Schematic of the global, induced flow through 3D neural constructs. Cells in 3D (neuronal cultures or neuronal–astrocytic co-cultures) were homogeneously dispersed throughout a 500–750 μm thick matrix (not to scale). To simplify the drawing, only three Au grids are shown at an arbitrary distance from the construct to facilitate the description. Note that the bottom of the construct actually rests on the perfusing substrate having embedded nine Au grids. Medium issuing closer to the perimeter of the engineered construct begins turning at lower elevations and vectoring towards the exit microchannels. Medium issuing near the center penetrates deeper into the construct and starts turning at higher elevations.

photomicrographs from 3D cultures are 50–100 μm thick reconstructions. General linear model ANOVA was used followed by post-hoc Tukey's pair-wise comparisons ($p < 0.05$ was required for significance in either test). Data are presented as mean±standard deviation.

Results

Perfusion platform microfluidic characterization

Velocity distributions were measured at the center of the perfused cell culture chamber (figure 4(a)) at a nominal flow rate of 11 μL min^{-1} where the flow was engendered by an array of microjets that emanate from the grids at the chamber base (figure 3). Measurements were taken in several planes that were parallel to the perfusing substrate and normal to the submerged microjets (and therefore resolve the spanwise velocity components normal to the axes of the jets). Data revealed that the dynamics of the induced flow was elevation dependent (figures 4(b)–(i)).

Immediately downstream of the grid (figure 4(b)), the flow was characterized by discharge of discrete, submerged, laminar microjets each having a nominal speed of 12 μm s^{-1} (Reynolds number $Re = 6 \times 10^{-4}$). The magnitude of the induced spanwise velocity was the lowest near the jet axes where their streamwise momentum peaked. With increasing distance from the grid openings, microjets began to interact with the lower momentum medium within the chamber. The momentum exchange through these shear-driven interactions induced motion and improved mixing in the surrounding fluid. Jets spread out laterally (broadened) and the magnitude of the induced spanwise velocity increased with elevation (figures 4(b), (c)). The broadening of the microjets was accompanied by a decrease in their streamwise momentum. Farther downstream from the perfusing substrate, broadening jets began to interact laterally with each other resulting in the overall reduction in their spanwise momentum (figures 4(d), (e)), the merging of jets and the loss of their coherence (figures 4(e)–(g)). By exploiting low *Re* jet-to-jet interactions, mixing within the chamber intensifies as the motions in surrounding fluid were effectively, convectively induced.

At higher elevations, peripheral perfusate withdrawal created significant 3D convection. Merged jet outflows began vectoring towards and leaving the chamber through microchannel exits (figures 4(h), (i)). This turning took place at higher elevations for the merged jet outflow near the center of the chamber than for the merged flow from the jets discharged closer to the chamber perimeter (figures 4(h), (i)). At sufficiently high flow rates, fluid near the center of the chamber that propagated deeper actually impinged on the membrane at the top of the chamber and formed a stagnation point. Developing wall jet (along the membrane surface) from that point on facilitated the radial turning of peripheral merged jet outflows towards the exits.

In summary, these observations support the truly 3D, theoretical flow profiles through the engineered cellular constructs previously shown (figure 3). Specific topologies of both the inflow and the outflow convectively augment mass transport through momentum exchange between the incoming (fresh), withdrawn (depleted), and medium within the chamber. Significant mixing enhancements were achieved through small-scale jet interactions and fluid shear.

Limitations in 3D cell density reliant on passive diffusion

We choose to establish viable cell density ranges and other culture parameters using neuron-only cultures based on the assumption that with the absence of glial support, neurons will require a more tightly regulated microenvironment (unpublished observations), thus being a more sensitive marker to establish effective fluidic parameters. Accordingly, we assessed neuronal survival in passive diffusion 3D culture for a range of cell densities (1250–12 500 cells mm^{-3}) at 2 and 7 DIV. Overall, cell viability depended significantly on plating density ($p < 0.001$), DIV ($p < 0.05$) as well as interactions

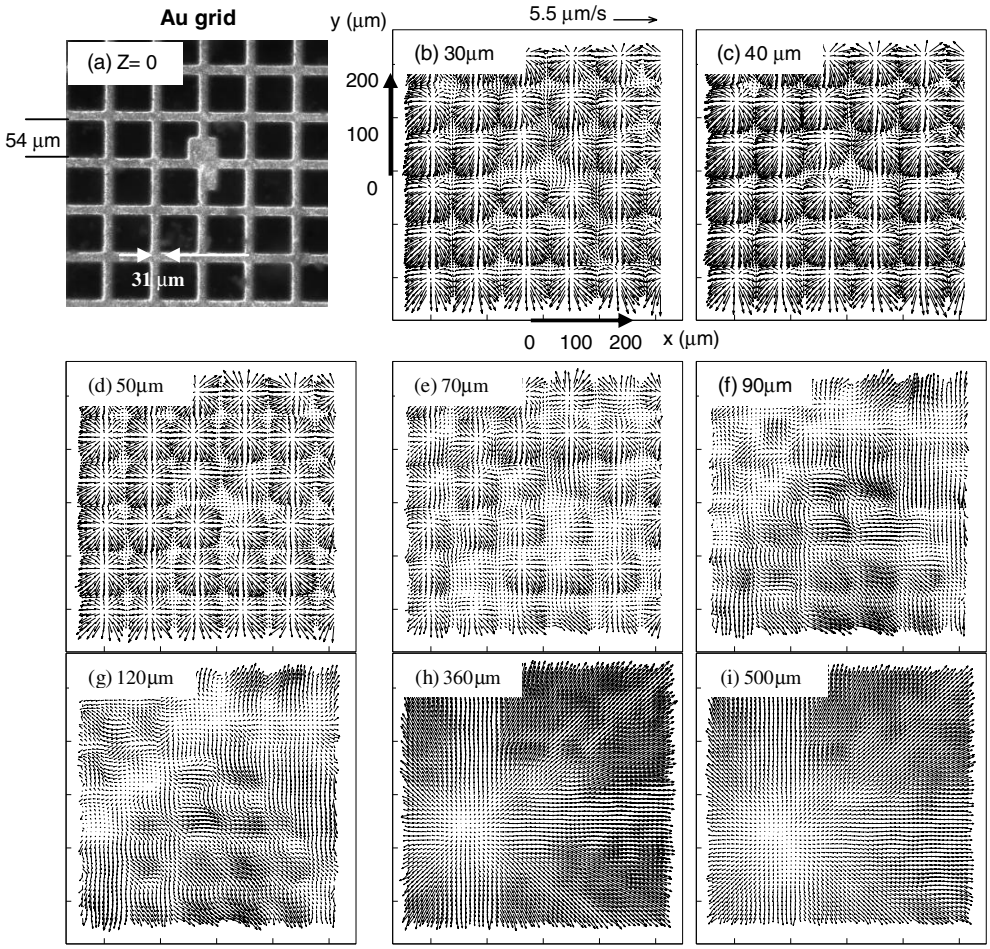

Figure 4. μPIV measurements at different elevations in planes parallel to the perfusing substrate: the field of view measures 450 × 457 μm and covers the central region of the center Au grid with an array of ∼5 × 5 square openings in focus (a); radial spreading of discrete, submerged, laminar microjets upon their discharge (b); microjet broadening upon their interaction with the low momentum medium within the chamber (c); a reduction in magnitude of the radial microjet velocity with further, increasing distance from the perfusing substrate (d); jet-to-jet interactions with the loss of symmetry (e)–(g); microjet outflows merge and begin vectoring towards the exit microchannels with peripheral microjets beginning to turn at lower elevations (h), (i).

between these factors ($p < 0.01$) (figure 5). Specifically, at 2 DIV, cells plated at $\leqslant$5000 cells mm^{-3} demonstrated relatively high viability; however, there was a significant reduction in survival at cell densities $\geqslant$6250 cells mm^{-3} ($p < 0.05$), suggesting that passive diffusion was insufficient to satisfy neuronal metabolic requirements at these increased cell densities. Interestingly, a parabolic response was observed in neuronal viability at 7 DIV, with cultures plated at $\leqslant$2500 cells mm^{-3} demonstrating poor viability in addition to higher cell density populations ($\geqslant$6250 cells mm^{-3}) exhibiting poor viability (<50% for each). The delayed neuronal death in low cell density 3D culture was likely independent of mass transport limitations. However, passive diffusion cultures plated at 3750–5000 cells mm^{-3} presented significantly higher viability than other cell density ranges ($p < 0.05$) at this time point. Moreover, this cell density range yielded cultures with extensive neurite arborization, demonstrating neuronal survival and active outgrowth under these culture parameters.

Continuous medium perfusion improves survival in neuronal cultures and neuronal–astrocytic co-cultures

The effects of continuous medium perfusion on the survival of high cell density, 3D neuronal cultures and neuronal–astrocytic co-cultures were assessed in comparison to non-perfused cultures. Survival depended significantly on culture type ($p < 0.01$) and perfusion rate ($p < 0.001$), with no significant interactions between these factors (figure 6). Specifically, by 2 days post-plating there was widespread degeneration and cell death in the majority of the non-perfused cultures, corroborating previous results demonstrating that passive diffusion-driven mass transport was not sufficient to support viable neural cultures at this combination of culture thickness ($\geqslant$500 μm) and cell density ($\geqslant 10^4$ cells mm^{-3}). As degeneration in the non-perfused cultures progressed, there became clusters of live and dead cells, although the majority of the cells and matrix were completely degraded. In non-perfused neuronal cultures and neuronal–astrocytic co-cultures, the remaining cell density was <20% of the initial cell density, and the mean thickness of the remaining matrix

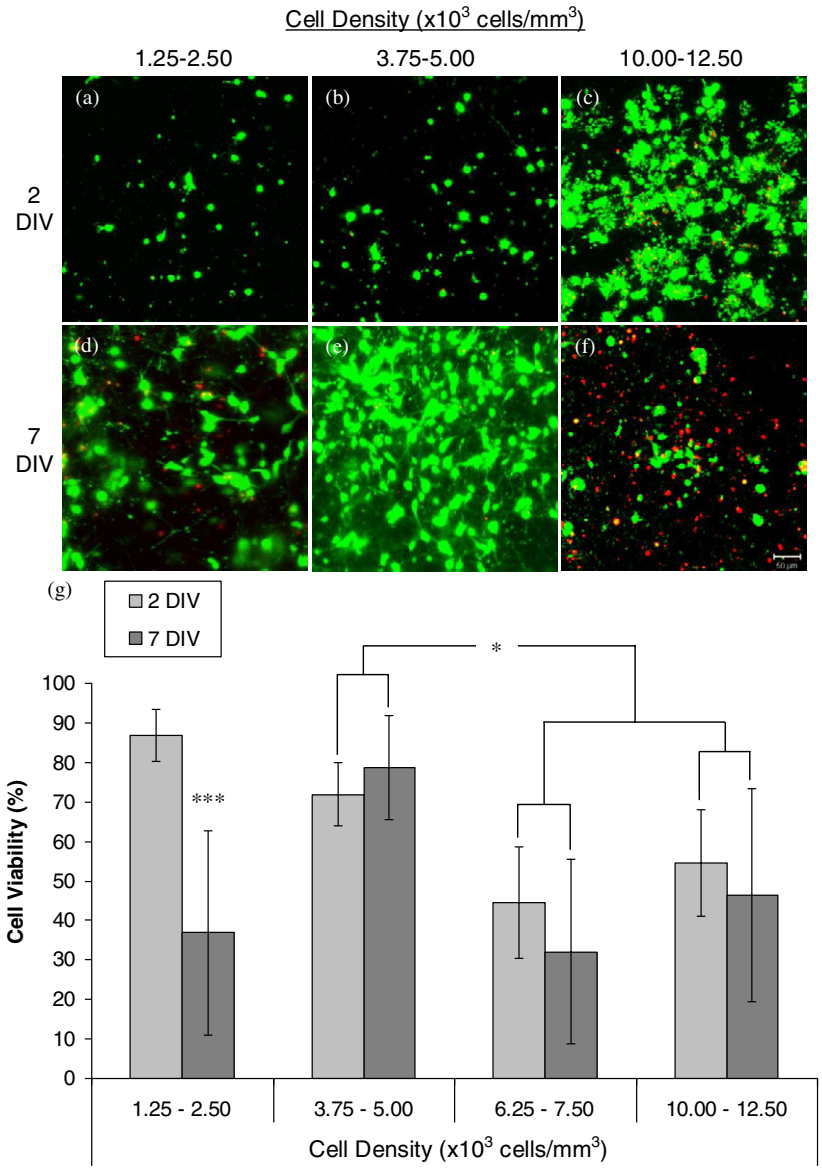

Figure 5. Neuronal survival depends on 3D cell density. Fluorescent confocal reconstructions of representative neuronal cultures plated at various cell densities. Cells were stained to discriminate live cells (green) and the nuclei of dead cells (red) at 2 DIV (a)–(c) and 7 DIV (d)–(f). The percentage of viable cells in 3D neuronal cultures varied significantly based on plating density; densities ranging from 6.25–12.50 $\times$ 10^3 cells mm^{-3} had significantly reduced viability versus 3.75–5.00 $\times$ 10^3 cells mm^{-3} at 2 and 7 DIV (* $p < 0.05$) (g), likely due to mass transport limitations in passive diffusion cultures. Also, the viability was significantly reduced at 7 DIV versus 2 DIV for cultures plated at 1.25–2.50 $\times$ 10^3 cells mm^{-3} (*** $p < 0.001$); this second wave of cell death may be due to insufficient neuron–neuron interactions. Scale bar = 50 μm; each reconstruction was from 100 μm thick z-stack.

was 52.7 $\pm$ 32.3 μm and 142.3 $\pm$ 93.1 μm, respectively, underscoring the extent of the cellular/matrix degradation. Additionally, this effect was particularly pronounced in the neuronal cultures compared to the neuronal–astrocytic co-cultures, as both viability and the cell density of remaining cells were significantly reduced ($p < 0.05$).

Continuous medium perfusion was found to attenuate culture degeneration and significantly enhance survival over a range of flow rates (2.0–11.0 μL min^{-1}) versus non-perfused cultures in both neuron-only cultures and neuronal–astrocytic co-cultures ($p < 0.01$) (figure 6). This range of perfusion rates produced neural cultures with the remaining cell density being $>10^4$ cells mm^{-3}, and these cultures exhibited widespread process outgrowth and the formation of 3D connectivity. Additionally, the highest perfusion rates evaluated (10.0–11.0 μL min^{-1}; corresponding to 25–27 medium exchanges per day) maintained overall culture viability at >90% in both neuron-only and neuronal–astrocytic co-cultures, demonstrating that convective enhancement in nutrient delivery substantially increased survival in high cell density 3D neural cultures.

Proximity to perfusion source influences survival

In high cell density, 3D neuronal–astrocytic co-cultures, viability was assessed as a function of distance from perfusion

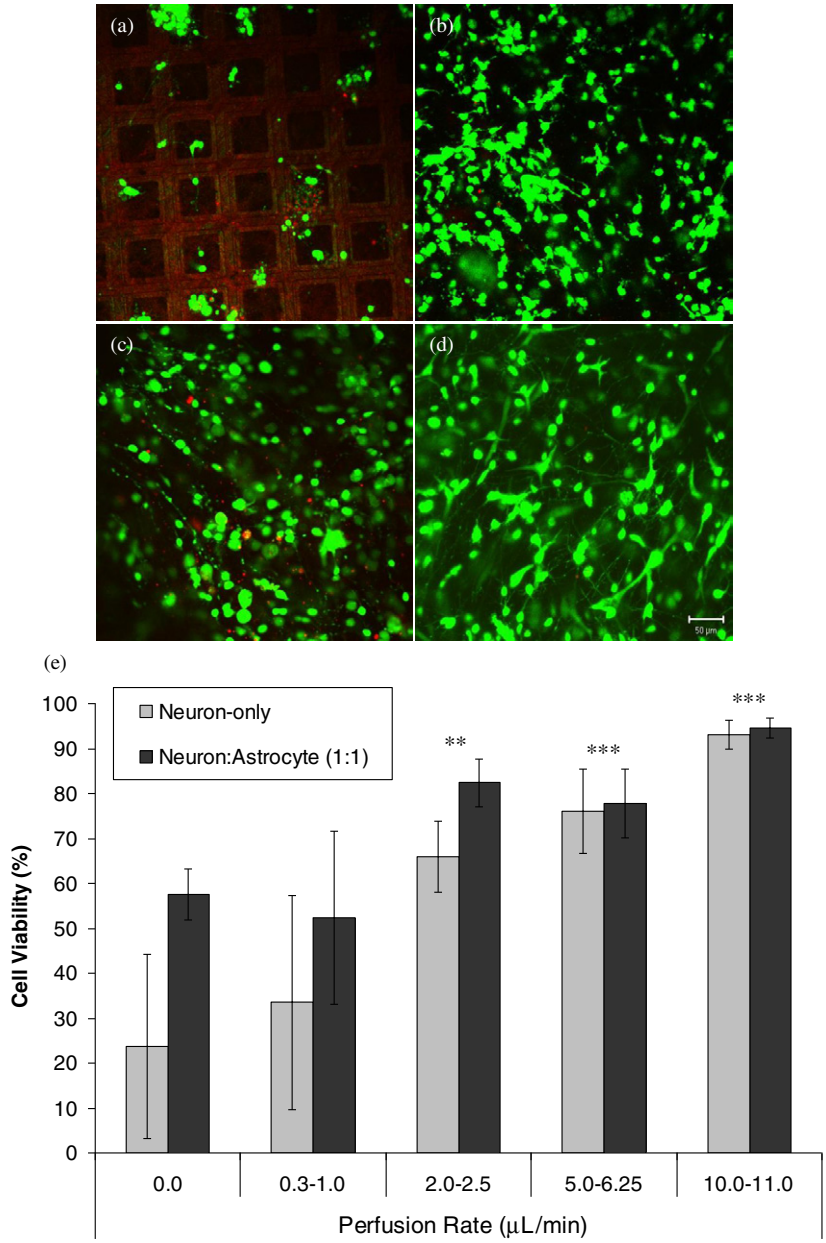

Figure 6. Neuronal and neuronal–astrocytic survival with continuous medium perfusion. Representative confocal reconstructions of 3D neural cultures stained to denote live cells (green) and the nuclei of dead cells (red). Increased cell density (10^4 cells mm^{-3}), thick ($\geqslant$500 μm) 3D neural cultures were plated with or without continuous medium perfusion. Neuronal cultures in 3D at 2 DIV either non-perfused (a) or perfused at a rate of 10.0–11.0 μL min^{-1} (b). Neuronal–astrocytic (1:1 ratio) co-cultures in 3D at 2 DIV either non-perfused (c) or perfused at a rate of 10.0–11.0 μL min^{-1} (d). Passive diffusion was insufficient to support thick 3D neural cultures at such high cell densities, as non-perfused (0.0 μL min^{-1}) cultures had widespread cell death and matrix degradation. Relatively high perfusion rates of 10.0–11.0 μL min^{-1} (corresponding to 25–27 medium exchanges per day) maintained culture viability at >90% in both neuron-only and neuronal–astrocytic co-cultures, demonstrating that convective enhancement of nutrient delivery can increase survival in high cell density neural cultures. Specifically, there was significant improvement in survival for perfusion rates of 2.0–2.5 μL min^{-1} (** $p < 0.01$), 5.0–6.25 μL min^{-1} (*** $p < 0.001$), and 10.0–11.0 μL min^{-1} (*** $p < 0.001$) compared to non-perfused cultures in both neuron-only cultures and neuronal–astrocytic co-cultures (e). Scale bar = 50 μm; reconstructions are from the middle of the cultures (50 μm thick z-stack).

source at perfusion rates of 2.50, 6.25 and 11.0 μL min^{-1} (figure 7). Across these perfusion groups, there were no significant differences in culture thickness or cell density, which were 498.0 $\pm$ 16.7 μm and 11.4 $\pm$ 4.8 $\times$ 10^3 cells mm^{-3}, respectively. However, cell survival was found to depend significantly on proximity to perfusion source ($p < 0.05$). Specifically, for lower flow rates of 2.5 and 6.25 μL min^{-1}, there was a significant reduction in viability at the top of the culture versus the bottom of the culture (closest to the perfusion inlet) ($p < 0.05$). However, this was not the case for the highest flow rate evaluated, 11.0 μL min^{-1}, where viability was constant across the thickness of the culture. A morphological analysis of cells in perfused cultures revealed stark morphological abnormalities based on perfusion rate

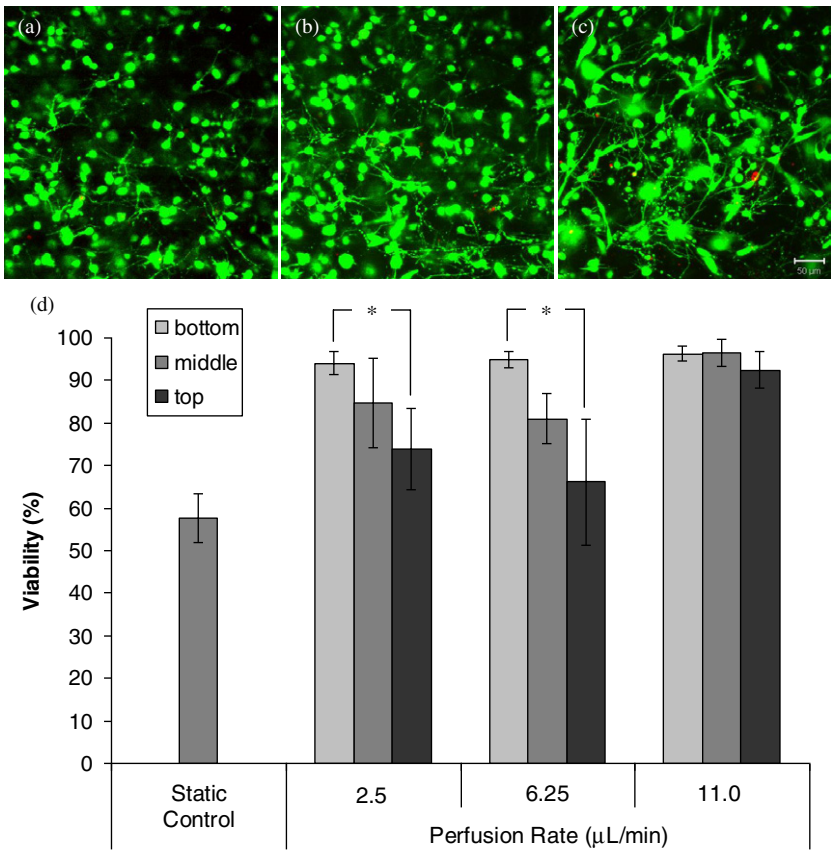

Figure 7. Culture viability as a function of distance from perfusion source. Representative confocal micrographs of a neuronal–astrocytic co-culture perfused at 6.25 μL min^{-1} with reconstructions from the bottom (closest to the perfusion source) (a), middle (b) and top (closest to the media bath) (c) of the co-culture. Survival depended on proximity to the perfusion source for lower flow rates (* $p < 0.05$); however, this effect was abolished at 11.0 μL min^{-1}, the highest perfusion rate evaluated. Scale bar = 50 μm; reconstructions from 50 μm thick z-stacks.

and distance from perfusion source, observations that may provide insight into cell death in this system (figure 8). Cells were observed to exhibit a degenerating morphology in the 2.5 μL min^{-1} and 6.25 μL min^{-1} cultures, most notably at the top of the cultures, as there were cells with punctated body formation and condensed nuclear material. The percentage of dead cells (EthD-1^{+}) exhibiting this specific degenerating morphology was quantified, revealing that neural cell degeneration depended significantly on the perfusion rate and distance from the perfusion source in the system ($p < 0.01$ and $p < 0.05$, respectively). There was a significant increase in the presence of this degenerating morphology at perfusion rates of 2.5 μL min^{-1} and 6.25 μL min^{-1} compared to 11.0 μL min^{-1} ($p < 0.05$ each). Additionally, within cultures perfused at 6.25 μL min^{-1}, there was a significant increase in the percentage of degenerating cells at the top versus the bottom of the culture ($p < 0.01$); however, this was not the case at 11 μL min^{-1}, where there was a paucity of degenerating cells, or at 2.5 μL min^{-1}, where the presence of degenerating cells was more consistent across the culture thickness. Thus, at lower flow rates or further distances from the perfusion source, the presence of such morphological alterations may indicate regions still lacking a sufficient amount of nutrients. However, these degenerating morphologies were rare in cultures perfused at 11.0 μL min^{-1}, providing further support that this perfusion rate was sufficient to satisfy the metabolic requirements for 3D neural cultures at this cell density across the full culture thickness.

Discussion and conclusions

We have developed a system for the support of thick, high cell density, 3D neuronal cultures and neuronal–astrocytic co-cultures using continuous medium perfusion. We initially established cell densities where passive diffusion was insufficient to meet cellular metabolic needs; however, it should be noted that limitations for passive diffusion to support cultures will likely depend on geometry as well (e.g., thickness, surface area to volume ratio). In our system, non-perfused neural cultures at this thickness ($\geqslant$500 μm) and cell density ($\geqslant 6.25 \times 10^3$ cells mm^{-3}) were found to undergo widespread degradation by 2 days post-plating, suggesting that cellular metabolic needs were not met by passive diffusion. Additionally, we observed a delayed cell death in low density 3D neuronal cultures (between 2 and 7 DIV), most likely not due to mass transport limitations but rather insufficient cell–cell support (Wang and Cynader 1999). The scope of the current work was to use convective intercellular enhancement to improve mass transport in high cell density 3D neural cultures; however, the mechanism of neuronal death in low density cultures merits follow-up. Additionally, in

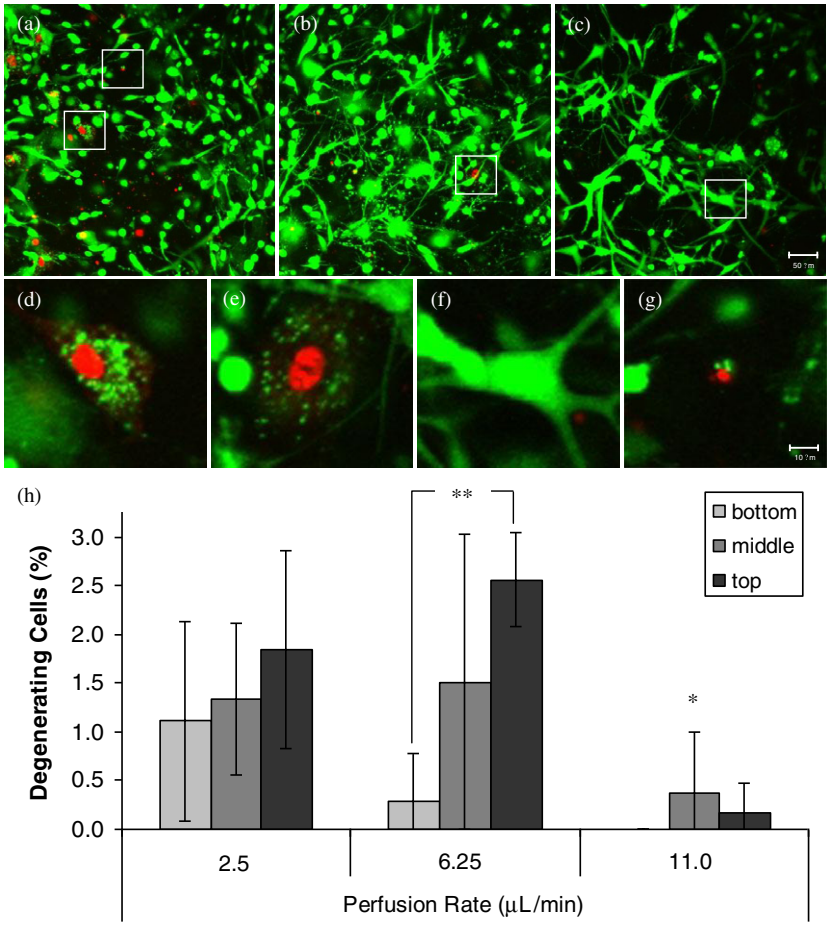

Figure 8. Morphology of dead cells. Top sections of perfused 3D co-cultures subjected to a flow rate of 2.5 μL min^{-1} (a), 6.25 μL min^{-1} (b) or 11.0 μL min^{-1} (c). Cells exhibiting a degenerating morphology were apparent for the 2.5 μL min^{-1} and 6.25 μL min^{-1} cultures (note punctated body formation and condensed nuclear material) ((d), (e)) in comparison to a healthy cell (f) or a dead cell without a swollen nucleus (g). The presence of degenerating cells may indicate inadequate nutrient delivery, and were most notably observed at positions furthest from the perfusion source. Conversely, such cells were rare in the 11.0 μL min^{-1} cultures, suggesting that metabolic requirements were satisfied at this highest flow rate. The percentage of dead cells (EthD-1^{+}) exhibiting this specific degenerating morphology was quantified (h). The percentage of dead cells presenting a degenerating morphology was significantly reduced at 11.0 μL min^{-1} compared to 2.5 μL min^{-1} and 6.25 μL min^{-1} perfusion rates (* $p < 0.05$). Additionally, within cultures perfused at 6.25 μL min^{-1}, there was a significant increase in the percentage of degenerating cells at the top versus the bottom of the culture (** $p < 0.01$); however, at the lower flow rate of 2.5 μL min^{-1}, degeneration did not vary with position from the perfusion source.

passive-diffusion cultures, survival was enhanced in neuronal–astrocytic co-cultures versus neuronal cultures, suggesting that there is an astrocytic role in improving neuronal survival and/or a broader range of parameters permitting astrocytic survival (Wang and Cynader 1999). Using our custom-made convective bioreactor system, continuous medium perfusion at flow rates in the range of 2.0–11.0 μL min^{-1} was found to attenuate culture degeneration and significantly improve survival in both neuronal cultures and neuronal–astrocytic co-cultures. Furthermore, the highest medium flow rates of 10.0–11.0 μL min^{-1} (corresponding to ∼15–16 mL/day or ∼25–27 exchanges/day) was found to maintain culture viability to a greater extent than the other flow rates evaluated.

The availability of nutrients via intercellular mass transport must surpass specific metabolic thresholds for 3D culture systems to support viable cells constructs (Cartmell *et al* 2003, Hongo *et al* 2005, Toh *et al* 2005)). The absence of functional vasculature to supply oxygen and nutrients to the tissue limits normal diffusion rates of metabolites, especially in thicker cultures. Functional replacement modes of mass transport depend on the cell density and culture geometric parameters, in addition to the diffusion/consumption characteristics of a particular compound (amongst potentially other factors). When characteristic culture dimensions exceed characteristic diffusive length scales, concentrations can differ drastically between regions of the 3D culture system. This may cause the part of the culture with the lowest concentration of nutrients to decay. When the dominant mode of mass transport is pure diffusion the extracellular concentrations of nutrients and other relevant agents may never reach equilibrium with the intercellular environment, and cultures eventually die. In acute slices, for example, the tissue decay rate may be slowed down by the use of commercially available incubation baths (Langmoen and Anderson 1981). However, inadequate, diffusion-limited nutrient availability and tissue oxygenation eventually leads to time-dependant metabolic run-down. The

quality of tissue perfusion, therefore, becomes the most important parameter limiting the survival of 3D *in vitro* neural preparations, whether slice or dense cultures. The goal of our system was to extend the viability of 3D cultures by maintaining high intercellular concentration of nutrients and gas, uniformly throughout the culture. Our approach was to provide convective enhancement in nutrient delivery to the culture by forcing the flow through the intercellular space. Although mass transport across the cellular membranes seemingly remains inherently diffusive, forced convection of the nutrient medium may obtain sufficiently high concentration of nutrients in the extracellular space throughout the culture thickness. That is, at high enough flow rates forced convection enables facile aerobic metabolism and eliminates temporally invariant concentration gradients otherwise associated with diffusive nutrient delivery. Even in the presence of convective pathways, however, low perfusion rates were found to be insufficient to overcome the concentration gradients as neural cells in dense 3D culture began to die. In the disclosed perfusion platform this was observed through lower culture viabilities with increasing distance from the perfusing substrate. However, at sufficiently high exchange rates, cultures remained healthy, while non-perfused cultures or cultures perfused at lower flow rates were shown to decay, thus corroborating the utility of forced convection perfusion over a purely diffusive intercellular transport mechanism.

In forced convection perfusion, cellular attachment to the perfusing substrate plays a pivotal role in the success and repeatability of viability measurements in perfused constructs. Poor adhesion creates pockets of low resistance domains that may hinder the media supply towards the interior of the culture where the resistance to the flow would be much higher, thereby depreciating the impact of predominantly convective mass transport. For our conditions, however, neural cultures adhered well to the perfusing substrate over time, even with the highest exchange rates examined. In addition to potential problems with adhesion, prohibitively high exchange rates can also lead to a reduction in concentration of substances secreted by the cells into their microenvironment, such as neurotrophins. Although this can be mitigated by the partial re-use of collected, spent perfusate, further increase in exchange rates, beyond minimum necessary to obtain $>90\%$ viability throughout the culture, is not only redundant in terms of expenses associated with the amount of spent media, but could potentially harm the cultures long-term. Specifically, high pressure gradients across the culture and/or high values of fluid shear stress exerted upon the cellular membranes could change morphology and ultimately injure the cultures (LaPlaca and Thibault 1997). Increases in 3D cell density raise nutritive and oxygen requirements, and demand an efficient removal of catabolic waste products. These requirements can only be met by the use of convective circulation to augment the cellular viability, but at higher values of the intercellular flow resistance. Therefore the limiting factor in neural construct cell density or thickness may be the magnitude of pressure gradient across the culture. Although cell density in the present experiments remains an order of magnitude lower than that found in various cortical regions (Gabbott and Stewart 1987, Braitenberg 2001), the utility of forced convection perfusion in permitting the survival of increased cell density engineered constructs was demonstrated. Perfusion chambers were optimized to support high density, 3D cultures while exceeding the available exchange rates of commercial devices by several orders of magnitude. Additionally, flow through the cells/matrix construct may create a distributed fluidic network for nutrient delivery that mimics a circulatory network. This microvasculature-like network, in combination with efficient, intercellular forced convection, may eliminate the need to microfabricate 3D scaffolds to support the construct and inject the nutrient medium at different elevations.

The results of these studies warrant follow-up using higher flow rates and longer experimental time points. Higher flow rates may further improve culture survival initially; conversely, the ability of the cells to regulate their microenvironment may decrease for high convective rates. Furthermore, neuronal maturation may influence optimal exchange rates over time. Neurons may better autoregulate at later time points, requiring lower convection rates to sustain high concentration of substances secreted by the cells to regulate their microenvironment. Long-term studies may therefore require temporal tuning of the cellular feeding schedule as a function of maturity and functional requirements, all features that are controllable with the perfusion system developed here.

The dynamics of the flow within the perfusion chambers was elevation dependent and changed from free flow of discrete jets upon their discharge from the openings to interactions among decelerating, broadening jets in peripherally biased perfusate extraction. Peripheral withdrawal created favorable, forced convection, intercellular circulation at higher elevations. This can be further improved by reducing the chamber height to match that of the actual culture thickness and/or by carefully adjusting the base position of the peripheral microchannel exits to promote cellular viability at higher elevations via significant convective enhancement in stagnation and wall jet regions.

The utility of forced convection perfusion and disclosed perfusion platform can be expanded beyond neurobiological applications. Simple fabrication methodology enables application-specific changes in the design and in the integration of additional functionalities (e.g., multielectrode arrays, biosensors, mixers, cell sorters) with a minimum turnaround time. Devices can be made as disposable cellular essays for use in pharmacological or biochemical analyses, cytophilic biomaterials research, haptotaxis or chemotaxis chambers (e.g. Dertinger *et al* (2001)). Microfabrication compatibility enables the development of specific cellular environments having adjustable shape, texture, protein adsorptivity, surface chemistry or tunable topography of extracellular matrices and chemically patterned microfabricated scaffolds that can only be realized in dynamic perfusion platforms utilizing forced convection to augment cellular viability. This custom neural bioreactor system may be utilized to controllably release modulatory compounds or inject selected agents in time-periodic or aperiodic fashion.

This work demonstrated the utility of forced convection perfusion to support thick, high cell density, 3D neuronal

cultures and neuronal–astrocytic co-cultures. We found that continuous nutrient delivery in custom-made perfusion chambers extends the viability of neural engineered constructs plated at 10^4 cells mm^{-3}. Extensive decay in non-perfused cultures corroborates the nutrient deficiency associated with purely diffusive intercellular mass transport. Perfused culture viability increased with the increase in convective exchange rates confirming that indeed convective intercellular mass transport ensures high nutrient concentration throughout the cultured construct, thus meeting or exceeding the metabolic thresholds at sufficiently high exchange rates. Specifically, at 25–27 convective exchanges per day, culture thickness was preserved with >90% viability throughout the thickness. *In vitro* models of neural cells have proven effective in the systematic identification of a range of neurobiological phenomena. The 3D model presented here maintains the advantages of traditional *in vitro* systems while more closely approximating the *in vivo* environment including but not limited to 3D cytoarchitecture, distribution of cell–cell/cell–matrix interactions and multicellular composition at a cell density approaching that of brain tissue. Next generation engineered 3D neural cell culture systems inspired by the CNS, which include heterogeneous cell populations, high cell densities and ECM constituents, may provide a powerful experimental framework for the systematic elucidation of neurobiological function in a controlled setting.

Acknowledgments

Financial support was provided by the National Institutes of Health Bioengineering Research Partnership (award no. EB00786).

References

Aschner M 2000 Neuron–astrocyte interactions: implications for cellular energetics and antioxidant levels *Neurotoxicology* **21** 1101–7

Bellamkonda R, Ranieri J P and Aebischer P 1995a Laminin oligopeptide derivatized agarose gels allow three-dimensional neurite extension in vitro *J. Neurosci. Res.* **41** 501–9

Bellamkonda R, Ranieri J P, Bouche N and Aebischer P 1995b Hydrogel-based three-dimensional matrix for neural cells *J. Biomed. Mater. Res.* **29** 663–71

Bolinder J 1999 On the accuracy of digital particle image velocimetry system *Technical Report* Lund Institute of Technology ISSN 0282–1990

Braitenberg V 2001 Brain size and number of neurons: an exercise in synthetic neuroanatomy *J. Comput. Neurosci.* **10** 71–7

Brewer G J 1995 Serum-free B27/neurobasal medium supports differentiated growth of neurons from the striatum, substantia nigra, septum, cerebral cortex, cerebellum, and dentate gyrus *J. Neurosci. Res.* **42** 674–83

Brewer G J, Torricelli J R, Evege E K and Price P J 1993 Optimized survival of hippocampal neurons in B27-supplemented Neurobasal, a new serum-free medium combination *J. Neurosci. Res.* **35** 567–76

Cartmell S H, Porter B D, Garcia A J and Guldberg R E 2003 Effects of medium perfusion rate on cell-seeded three-dimensional bone constructs in vitro *Tissue Eng.* **9** 1197–203

Chen J P and Lin C T 2006 Dynamic seeding and perfusion culture of hepatocytes with galactosylated vegetable sponge in packed-bed bioreactor *J. Biosci. Bioeng.* **102** 41–5

Choi H K, Won L and Heller A 1993 Dopaminergic neurons grown in three-dimensional reaggregate culture for periods of up to one year *J. Neurosci. Methods* **46** 233–44

Coates P W, Fermini B, Strahlendorf J C and Strahlendorf H K 1992 Utilization of three-dimensional culture for early morphometric and electrophysiological analyses of solitary cerebellar neurons *Dev. Neurosci.* **14** 35–43

Coates P W and Nathan R D 1987 Feasibility of electrical recordings from unconnected vertebrate CNS neurons cultured in a three-dimensional extracellular matrix *J. Neurosci. Methods* **20** 203–10

Cooper J A Jr, Li W J, Bailey L O, Hudson S D, Lin-Gibson S, Anseth K S, Tuan R S and Washburn N R 2007 Encapsulated chondrocyte response in a pulsatile flow bioreactor *Acta Biomater.* **3** 13–21

Croning M D and Haddad G G 1998 Comparison of brain slice chamber designs for investigations of oxygen deprivation in vitro *J. Neurosci. Methods* **81** 103–11

Cukierman E, Pankov R, Stevens D R and Yamada K M 2001 Taking cell-matrix adhesions to the third dimension *Science* **294** 1708–12

Cukierman E, Pankov R and Yamada K M 2002 Cell interactions with three-dimensional matrices *Curr. Opin. Cell Biol.* **14** 633–9

Cullen D K, Vukasinovic J, Irons H R, Glezer A, Wheeler B C and LaPlaca M C 2006 Engineered high cell density three-dimensional constructs *Society for Neuroscience Annual Fall Meeting (Altanta, GA)*

Dertinger S K W, Chiu D T, Jeon N L and Whitesides G M 2001 Generation of gradients having complex shapes using microfluidic networks *Anal. Chem.* **73** 1240–6

Fawcett J W, Barker R A and Dunnett S B 1995 Dopaminergic neuronal survival and the effects of bFGF in explant, three dimensional and monolayer cultures of embryonic rat ventral mesencephalon *Exp. Brain Res.* **106** 275–82

Fawcett J W, Housden E, Smith-Thomas L and Meyer R L 1989 The growth of axons in three-dimensional astrocyte cultures *Dev. Biol.* **135** 449–58

Gabbott P L and Stewart M G 1987 Distribution of neurons and glia in the visual cortex (area 17) of the adult albino rat: a quantitative description *Neuroscience* **21** 833–45

Gomes M E, Sikavitsas V I, Behravesh E, Reis R L and Mikos A G 2003 Effect of flow perfusion on the osteogenic differentiation of bone marrow stromal cells cultured on starch-based three-dimensional scaffolds *J. Biomed. Mater Res.* A **67** 87–95

Granet C, Laroche N, Vico L, Alexandre C and Lafage-Proust M H 1998 Rotating-wall vessels, promising bioreactors for osteoblastic cell culture: comparison with other 3D conditions *Med. Biol. Eng. Comput.* **36** 513–9

Grinnell F 2000 Fibroblast-collagen-matrix contraction: growth-factor signalling and mechanical loading *Trends Cell Biol.* **10** 362–5

Haas H L, Schaerer B and Vosmansky M 1979 A simple perfusion chamber for the study of nervous tissue slices in vitro *J. Neurosci. Methods* **1** 323–5

Holtorf H L, Jansen J A and Mikos A G 2005 Flow perfusion culture induces the osteoblastic differentiation of marrow stroma cell-scaffold constructs in the absence of dexamethasone *J. Biomed. Mater Res.* A **72** 326–34

Hongo T, Kajikawa M, Ishida S, Ozawa S, Ohno Y, Sawada J, Umezawa A, Ishikawa Y, Kobayashi T and Honda H 2005 Three-dimensional high-density culture of HepG2 cells in a 5-ml radial-flow bioreactor for construction of artificial liver *J. Biosci. Bioeng.* **99** 237–44

Hsiang J, Heller A, Hoffmann P C, Mobley W C and Wainer B H 1989 The effects of nerve growth factor on the development of septal cholinergic neurons in reaggregate cell cultures *Neuroscience* **29** 209–23

Kitagawa T, Yamaoka T, Iwase R and Murakami A 2006 Three-dimensional cell seeding and growth in radial-flow perfusion bioreactor for in vitro tissue reconstruction *Biotechnol. Bioeng.* **93** 947–54

Kleinman H K, McGarvey M L, Hassell J R, Star V L, Cannon F B, Laurie G W and Martin G R 1986 Basement membrane complexes with biological activity *Biochemistry* **25** 312–8

Langmoen T A and Andersen P 1981 The hippocampal slice *in vitro Electrophysiology of Isolated Mammalian CNS preparations* ed G A Kerkut and H V Wheal (London: Academic) p 51

LaPlaca M C and Thibault L E 1997 An in vitro traumatic injury model to examine the response of neurons to a hydrodynamically-induced deformation *Ann. Biomed. Eng.* **25** 665–77

Li C L and McIlwain H 1957 Maintenance of resting membrane potentials in slices of mammalian cerebral cortex and other tissues in vitro *J. Physiol.* **139** 178–90

McCarthy K D and de Vellis J 1980 Preparation of separate astroglial and oligodendroglial cell cultures from rat cerebral tissue *J. Cell Biol.* **85** 890–902

McDonald J, Chabinyc M, Metallo S, Anderson J, Stroock A and Whitesides G 2002 Prototyping of microfluidic devices in poly(dimethylsiloxane) using solid-object printing *Anal. Chem.* **74** 1537–45

McDonald J, Duffy D, Anderson J, Chiu D, Wu H, Schueller O and Whitesides G 2000 Fabrication of microfluidic systems in poly(dimethylsiloxane) *Electrophoresis* **21** 27–40

Meinhart C, Wereley S and Gray M 2000a Volume illumination for two-dimensional particle image velocimetry *Meas. Sci. Technol.* **11** 809–14

Meinhart C, Wereley S and Santiago J 2000b A PIV algorithm for estimating time-averaged velocity fields *Trans. ASME, J. Fluid Eng.* **122** 285–9

Nicoll R A and Alger B E 1981 A simple chamber for recording from submerged brain slices *J. Neurosci. Methods* **4** 153–6

O'Connor S M, Andreadis J D, Shaffer K M, Ma W, Pancrazio J J and Stenger D A 2000 Immobilization of neural cells in three-dimensional matrices for biosensor applications *Biosens. Bioelectron.* **14** 871–81

O'Connor S M, Stenger D A, Shaffer K M and Ma W 2001 Survival and neurite outgrowth of rat cortical neurons in three-dimensional agarose and collagen gel matrices *Neurosci. Lett.* **304** 189–93

O'Shaughnessy T J, Lin H J and Ma W 2003 Functional synapse formation among rat cortical neurons grown on three-dimensional collagen gels *Neurosci. Lett.* **340** 169–72

Potter S M and DeMarse T B 2001 A new approach to neural cell culture for long-term studies *J. Neurosci. Methods* **110** 17–24

Reynaud J C, Martini F, Chatel C, Buclin M, Raggenbass M and Puizillout J J 1995 A new interface chamber for the study of mammalian nervous tissue slices *J. Neurosci. Methods* **58** 203–8

Saini S and Wick T M 2003 Concentric cylinder bioreactor for production of tissue engineered cartilage: effect of seeding density and hydrodynamic loading on construct development *Biotechnol. Prog.* **19** 510–21

Santiago J, Wereley S, Meinhart C, Beebe D and Adrian R 1998 A particle image velocimetry system for microfluidics *Exp. Fluids* **25** 316–9

Schmeichel K L and Bissell M J 2003 Modeling tissue-specific signaling and organ function in three dimensions *J. Cell Sci.* (Pt 12) **116** 2377–88

Shi W X and Bunney B S 1990 A small volume chamber for electrical recording from submerged brain slices and a pulse-free medium supply system using a peristalic pump *J. Neurosci. Methods* **35** 235–40

Spector D H, Boss B D and Strecker R E 1993 A model three-dimensional culture system for mammalian dopaminergic precursor cells: application for functional intracerebral transplantation *Exp. Neurol.* **124** 253–64

Toh Y C, Ng S, Khong Y M, Samper V and Yu H 2005 A configurable three-dimensional microenvironment in a microfluidic channel for primary hepatocyte culture *Assay Drug Dev. Technol.* **3** 169–76

Tsacopoulos M 2002 Metabolic signaling between neurons and glial cells: a short review *J. Physiol. Paris* **96** 283–8

Tsacopoulos M and Magistretti P J 1996 Metabolic coupling between glia and neurons *J. Neurosci.* **16** 877–85

van den Dolder J, Bancroft G N, Sikavitsas V I, Spauwen P H, Jansen J A and Mikos A G 2003 Flow perfusion culture of marrow stromal osteoblasts in titanium fiber mesh *J. Biomed. Mater Res.* A **64** 235–41

Vukasinovic J and Glezer A 2006a Centimeter-scale diagnostics incubator with integrated perfusion *Proc. 10th Int. Conf. on Miniaturized Systems for Chemistry and Life Sciences*

Vukasinovic J and Glezer A 2006b A microfluidic perfusion chamber for neuronal cultures *Proc. of Bioengineering Conf.*

Wang F, Weaver V M, Petersen O W, Larabell C A, Dedhar S, Briand P, Lupu R and Bissell M J 1998 Reciprocal interactions between beta1-integrin and epidermal growth factor receptor in three-dimensional basement membrane breast cultures: a different perspective in epithelial biology *Proc. Natl Acad. Sci. USA* **95** 14821–6

Wang J, Asou Y, Sekiya I, Sotome S, Orii H and Shinomiya K 2006 Enhancement of tissue engineered bone formation by a low pressure system improving cell seeding and medium perfusion into a porous scaffold *Biomaterials* **27** 2738–46

Wang X F and Cynader M S 1999 Effects of astrocytes on neuronal attachment and survival in a serum-free co-culture system *Brain Res. Brain Res. Protoc.* **4** 209–16

Wang Y, Uemura T, Dong J, Kojima H, Tanaka J and Tateishi T 2003 Application of perfusion culture system improves in vitro and in vivo osteogenesis of bone marrow-derived osteoblastic cells in porous ceramic materials *Tissue Eng.* **9** 1205–14

Wereley S and Meinhart C 2004 *Diagnostic Techniques in Microfluidics* (New York: Springer)

Whitesides G, Ostuni E, Takayama S, Jiang X and Ingber D 2001 Soft lithography in biology and biochemistry *Annu. Rev. Biomed. Eng.* **3** 335–73

Woerly S, Plant G W and Harvey A R 1996 Cultured rat neuronal and glial cells entrapped within hydrogel polymer matrices: a potential tool for neural tissue replacement *Neurosci. Lett.* **205** 197–201

Xia Y and Whitesides G 1998 Soft lithography *Angew. Chem. Int. Ed.* **37** 551–75

Yamada K M, Pankov R and Cukierman E 2003 Dimensions and dynamics in integrin function *Braz. J. Med. Biol. Res.* **36** 959–66

Zbicz K L and Weight F F 1985 Transient voltage and calcium-dependent outward currents in hippocampal CA3 pyramidal neurons *J. Neurophysiol.* **53** 1038–58